IV International Conference on Simulation for Additive Manufacturing
Sim-AM 2023
E. Rank and S. Kollmannsberger (Eds)

MULTI-SCALE TOPOLOGY OPTIMIZATION OF BODIES WITH TPMS-BASED LATTICE STRUCTURES AND MORTAR CONTACT INTERFACES

N. STRÖMBERG

Department of Mechanical Engineering
School of Science and Technology
Örebro University
SE-701 82 Örebro, Sweden
e-mail: niclas.stromberg@oru.se, web page: http://www.oru.se

Key words: Topology optimization, TPMS-based lattices, Mortar contacts

Abstract. The combination of topology optimization, lattice structures and 3D printing has quickly emerged as a potential alternative for the design and manufacturing of lightweight components. However, the size of the building chamber restricts the size of this kind of lightweight designs. A possibility to overcome this limitation is to design assemblies of 3D printed lightweight components put together with contact interfaces. To design such an optimal lightweight assembly, the components should not be optimized separately, but the whole assembly should be optimized simultaneously with all components including their unilateral contact interfaces. This is the topic of the following work. In this paper, a framework for multi-scale topology optimization of assemblies of bodies with triply periodic minimal surfaces (TPMS)-based lattice structures and unilateral contact interfaces is developed and implemented in 3D. The contact interfaces are formulated for finite element bodies with non-matching meshes using the mortar approach which in turn is solved by the augmented Lagrangian formulation and Newton's method. The multi-scale topology optimization formulation, suggested in [1], is set up by defining two density variables for each finite element: one macro density variable governed by RAMP (Rational Approximation of Material Properties), and a micro density variable governed by representative orthotropic elastic properties obtained by numerical finite element homogenization of representative volume elements of the TPMS-based lattice structure. Thus, the macro density variable defines if an element should be treated as a void or be filled with lattice structure, and the micro density variable sets the local grading of the lattice. The potential energy of the system is maximized with respect to the design variables, in such manner no extra adjoint equation is needed for the sensitivity analysis. Both density variables are treated with a density filter, and the macro density variable is also passed a Heaviside filter. The final optimal assembly design is realized by transforming the optimal density fields to implicit surface-based geometries using a support vector machine and Shepard's interpolation method, which then can be 3D printed as the corresponding stl-file obtained by applying the marching cube algorithm. The implemented framework is demonstrated for three-dimensional benchmark problems.

1 INTRODUCTION

Recently, a framework for multi-scale topology optimization of TPMS-based lattice structures was presented in [1]. In this paper, unilateral contact is included in this framework by adopting a mortar approach, se e.g. [2]. In such manner, topology optimization of assemblies of bodies with non-matching meshes can be performed efficiently. Topology optimization is very sensitive to the set up of the boundary conditions. Therefore, if contact interfaces between bodies in an assembly is not handle properly, the design generated by the topology optimization might be far from optimal. In design for additive manufacturing, this might be an issue when an assembly of 3D printed components is designed. In this work, such contact interfaces between bodies are formulated using an augmented Lagrangian formulation where non-matching meshes are taken care by a mortar approach. The derived state problem is then solved using a non-smooth Newton method [3]. In [4], frictional impact and rolling were solved using this Newton approach, and frictional heating in disc pad system was considered using this method in [5]. The potential energy used in the derivation of the state problem is maximized in the topology optimization formulation. For zero prescribed displacements and zero initial contact gaps, this corresponds to minimizing the compliance. The main advantage of maximizing the potential energy is that no extra adjoint equation needs to be solved in the sensitivity analysis, which improves the numerical performance significantly. Topology optimization with unilateral contact can be found in e.g. [6, 7].

The outline of the paper is the following: in section 2, the governing equations are presented, in section 3, details about the mortar approach is revealed, in section 4, the topology optimization formulation is discussed, in section 5, a lightweight rocker arm with Schwarz-D lattice structures is optimized, and, finally, some concluding remarks are presented.

2 GOVERNING EQUATIONS

The potential energy of the assembly of bodies reads

$$\Pi(\boldsymbol{\rho}, \boldsymbol{\gamma}, \boldsymbol{d}) = \frac{1}{2}\boldsymbol{d}^T \boldsymbol{K}(\boldsymbol{\rho}, \boldsymbol{\gamma})\boldsymbol{d} - \boldsymbol{F}^T \boldsymbol{d}, \tag{1}$$

where $\boldsymbol{d}$ is the nodal displacement vector, $\boldsymbol{F}$ is the external force vector and

$$\boldsymbol{K} = \boldsymbol{K}(\boldsymbol{\rho}, \boldsymbol{\gamma}) = \bigcap_e \frac{\rho_e}{1 + n(1 - \rho_e)} \boldsymbol{k}_e(\gamma_e) \tag{2}$$

is the global stiffness matrix depending on macro element densities collected in $\boldsymbol{\rho} = \{0 < \epsilon \leq \rho_e \leq 1\}$ and the local relative element densities of the lattice $\boldsymbol{\gamma} = \{0 < l_b \leq \gamma_e \leq u_b \leq 1\}$, where ϵ is a small number, l_b and u_b are prescribed lower and upper limits on the relative lattice density γ_e, respectively. Furthermore, $\bigcap$ represents an assembly operator, n is the RAMP factor [8] and $\boldsymbol{k}_e = \boldsymbol{k}_e(\gamma_e)$ is the local element stiffness matrix for element e, which in turn is governed by the effective elastic properties of the TPMS-based lattice structure obtained by numerical homogenization, see [9].

The effective elastic properties are formulated using Voigt notation as

$$\boldsymbol{C}_e = \boldsymbol{C}_e(\gamma_e) = \begin{bmatrix} f_{11}c_{11} & f_{21}c_{21} & f_{31}c_{31} & 0 & 0 & 0 \\ f_{21}c_{21} & f_{22}c_{11} & f_{32}c_{31} & 0 & 0 & 0 \\ f_{31}c_{31} & f_{32}c_{31} & f_{33}c_{33} & 0 & 0 & 0 \\ 0 & 0 & 0 & f_{44}c_{44} & 0 & 0 \\ 0 & 0 & 0 & 0 & f_{55}c_{44} & 0 \\ 0 & 0 & 0 & 0 & 0 & f_{66}c_{66} \end{bmatrix}, \tag{3}$$

where $f_{ij} = f_{ij}(\gamma_e)$ are material interpolation laws obtained by the numerical homogenization approach presented in [9] and c_{ij} are the transversely isotropic elastic properties for the bulk material, i.e. $\boldsymbol{C} = \boldsymbol{C}_e(1)$, where

$$\boldsymbol{C}^{-1} = \begin{bmatrix} 1/E & -\nu/E & -\nu_{13}/E & 0 & 0 & 0 \\ -\nu/E & 1/E & -\nu_{13}/E & 0 & 0 & 0 \\ -\nu_{13}/E & -\nu_{13}/E & 1/E_{33} & 0 & 0 & 0 \\ 0 & 0 & 0 & 1/G_{23} & 0 & 0 \\ 0 & 0 & 0 & 0 & 1/G_{23} & 0 \\ 0 & 0 & 0 & 0 & 0 & 2(1+\nu)/E \end{bmatrix}. \tag{4}$$

The prescribed displacements are represented by

$$\boldsymbol{D}\boldsymbol{d} - \boldsymbol{\delta} = \boldsymbol{0}, \tag{5}$$

where $\boldsymbol{D}$ is a matrix representing orientations of the prescribed displacements collected in $\boldsymbol{\delta}$.

The unilateral contact conditions of the non-matching meshes are given by

$$\boldsymbol{C}_S\boldsymbol{d} + \boldsymbol{C}_M\boldsymbol{d} - \boldsymbol{g} \leq \boldsymbol{0}, \tag{6}$$

where $\boldsymbol{g}$ contains intial gaps, and $\boldsymbol{C}_S$ and $\boldsymbol{C}_M$ are the mortar normal transformation matrices which are derived by starting from the virtual power in the next section.

For given density distributions $\boldsymbol{\rho} = \hat{\boldsymbol{\rho}}$ and $\boldsymbol{\gamma} = \hat{\boldsymbol{\gamma}}$, the state of static equilibrium is obtained by solving

$$\begin{aligned} &\min_{\boldsymbol{d}} \Pi(\hat{\boldsymbol{\rho}}, \hat{\boldsymbol{\gamma}}, \boldsymbol{d}) \\ &\text{s.t.} \begin{cases} \boldsymbol{D}\boldsymbol{d} - \boldsymbol{\delta} = \boldsymbol{0}, \\ \boldsymbol{C}_S\boldsymbol{d} + \boldsymbol{C}_M\boldsymbol{d} - \boldsymbol{g} \leq \boldsymbol{0}. \end{cases} \end{aligned} \tag{7}$$

The corresponding Karush-Kuhn-Tucker (KKT) conditions read

$$\begin{aligned} \boldsymbol{K}\boldsymbol{d} - \boldsymbol{F} + \boldsymbol{D}^T\boldsymbol{\kappa} + \boldsymbol{C}_S^T\boldsymbol{\lambda} + \boldsymbol{C}_M^T\boldsymbol{\lambda} &= \boldsymbol{0}, \\ \boldsymbol{D}\boldsymbol{d} - \boldsymbol{\delta} &= \boldsymbol{0}, \\ \boldsymbol{\lambda} &\geq \boldsymbol{0}, \\ \boldsymbol{C}_S\boldsymbol{d} + \boldsymbol{C}_M\boldsymbol{d} - \boldsymbol{g} &\leq \boldsymbol{0}, \\ \boldsymbol{\lambda} \circ (\boldsymbol{C}_S\boldsymbol{d} + \boldsymbol{C}_M\boldsymbol{d} - \boldsymbol{g}) &= \boldsymbol{0}. \end{aligned} \tag{8}$$

Here, $\boldsymbol{\kappa}$ is a vector of Lagrange multipliers, which can be interpreted as the reaction forces to enforce the prescribed displacements in (5). Furthermore, $\boldsymbol{\lambda}$ contains mortar contact forces,

which are governed by the three latter constraints in (8) also known as Signorini's contact conditions. The system of equations and constraints in (8) is solved using the augmented Lagrangian approach and a non-smooth Newton method [3], where details are presented in the next section. By solving (8), we can obtain $\boldsymbol{d}$, $\boldsymbol{\kappa}$ and $\boldsymbol{\lambda}$ as implicit functions of $\boldsymbol{\rho}$ and $\boldsymbol{\gamma}$, i.e. $\boldsymbol{d} = \boldsymbol{d}(\boldsymbol{\rho}, \boldsymbol{\gamma})$, $\boldsymbol{\kappa} = \boldsymbol{\kappa}(\boldsymbol{\rho}, \boldsymbol{\gamma})$ and $\boldsymbol{\lambda} = \boldsymbol{\lambda}(\boldsymbol{\rho}, \boldsymbol{\gamma})$. This is utilized in section 4, when the nested formulation of the topology optimization problem is presented.

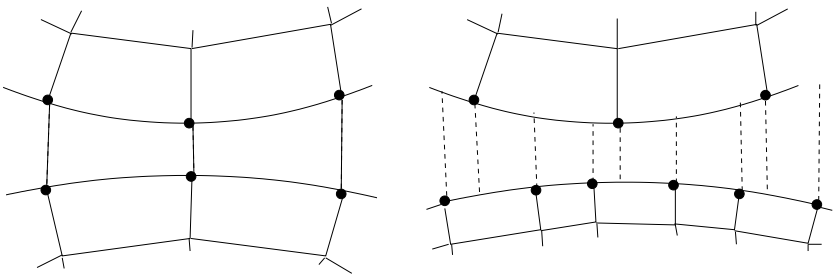

Figure 1: Examples of matching and non-matching meshes of a contact interface.

3 THE MORTAR CONTACT FORMULATION

Contact between deformable bodies with non-matching meshes as shown to the right in Figure 1 can efficiently be treated by applying the mortar approach, see e.g. [2]. The mortar approach is briefly presented here in a setting of small displacements. In the case of small displacements, the potential contact zone is identified by two contact surfaces Γ_c^i that are almost coinciding, i.e. $\Gamma_c^1 \approx \Gamma_c^2$. Γ_c^1 belongs to the first body Ω^1 (slave body) and Γ_c^2 is a part of the second one Ω^2 (master body). The virtual power of the total contact pressure $\boldsymbol{p}$ on this potential contact zone is defined by

$$\mathcal{P}_{\text{int}}^p = \int_{\Gamma_c^1} \boldsymbol{p} \cdot \boldsymbol{w}^1 \, \mathrm{d}A - \int_{\Gamma_c^2} \boldsymbol{p} \cdot \boldsymbol{w}^2 \mathrm{d}A, \tag{9}$$

where $\boldsymbol{w}^i$ denotes the virtual velocity field of respectively body. Since, $\Gamma_c = \Gamma_c^1 \approx \Gamma_c^2$, (9) can also be written more compactly as

$$\mathcal{P}_{\text{int}}^p = \int_{\Gamma_c} p_i(\boldsymbol{w}_i^1 - \boldsymbol{w}_i^2) \, \mathrm{d}A. \tag{10}$$

By introducing the normal contact pressure p_n and assuming that the tangential forces are zero, we can rewrite (10) to

$$\mathcal{P}_{\text{int}}^p = \int_{\Gamma_c} p_n(\boldsymbol{w}_i^1 - \boldsymbol{w}_i^2) n_i \, \mathrm{d}A, \tag{11}$$

where n_i represents the outward unit normal of the slave surface Γ_c^1.

The finite element discretization of (11) is done by introducing the following approximations:

$$\begin{aligned} p_n &= \sum_{A=1}^{n} N^A \lambda^A, \\ w_i^1 &= \sum_{A=1}^{n} N^A c_i^A, \\ w_i^2 &= \sum_{A=1}^{m} M^A c_i^A. \end{aligned} \tag{12}$$

Here, $N^A = N^A(\boldsymbol{x})$ represents the shape functions on Γ_c^1, which are taken to be the corresponding trace functions of the global shape functions on Ω^1. The total number of shape functions N^A on Γ_c^1 is n. In a similar way, $M^A = M^A(\boldsymbol{x})$ represents the shape functions on Γ_c^2, which are taken to be m in number. By inserting (12) into (11), one gets

$$\mathcal{P}_{\text{int}}^p = \sum_{A=1}^{n}\sum_{B=1}^{n} \int_{\Gamma_c} N^A N^B n_i \,\mathrm{d}A \lambda^A c_i^B - \sum_{A=1}^{n}\sum_{B=1}^{m} \int_{\Gamma_c} N^A M^B n_i \,\mathrm{d}A \lambda^A c_i^B, \tag{13}$$

or written as

$$\mathcal{P}_{\text{int}}^p = \sum_{A=1}^{n}\sum_{B=1}^{n} C_{Si}^{AB} \lambda^A c_i^B + \sum_{A=1}^{n}\sum_{B=1}^{m} C_{Mi}^{AB} \lambda^A c_i^B, \tag{14}$$

where

$$\begin{aligned} C_{Si}^{AB} &= \int_{\Gamma_c} N^A N^B n_i \,\mathrm{d}A, \\ C_{Mi}^{AB} &= -\int_{\Gamma_c} N^A M^B n_i \,\mathrm{d}A. \end{aligned} \tag{15}$$

The latter integral is known as the mortar integral. It is tricky to solve this integral because it cannot in general be dived into subdomains defined by the finite elements depending on the non-matching meshes. One way of fixing this problem is to us a quadrature rule with many integration points such as the Lobatto rule with 10 points presented in Table 1.

Table 1: *Lobatto rule with n_{int}=10 integration points.*

n_{int}	ξ_i	W_i
10	±0.1652789577	0.3275397612
	±0.4779249498	0.2920426836
	±0.7387738651	0.2248894320
	±0.9195339082	0.1333059908
	±1	0.0222222222

Assuming that the bodies Ω^i are linear elastic, using (14) in the finite element discretization of the global weak formulation, then one recovers the equilibrium equation in (8), where $\boldsymbol{C}_S$ and $\boldsymbol{C}_M$ contain (15).

In addition, if one assumes that Signorini's contact conditions hold, then these can be formulated by the following variational inequality: find $p_n \geq 0$ such that

$$\int_{\Gamma_c} (u_i^1 n_i - u_i^2 n_i - g)(q_n - p_n)\,\mathrm{d}A \leq 0 \quad \forall q_n \geq 0. \tag{16}$$

By inserting the finite element approximations of the displacements u_i^1 and u_i^2, and the contact forces q_n and p_n, (16) can be written as

$$\lambda^B \geq 0: \qquad \sum_{B=1}^{n} \delta^B(\gamma^B - \lambda^B) \leq 0 \quad \gamma^B \geq 0, \tag{17}$$

where

$$\delta^B = \sum_{A=1}^{n} \left(\int_{\Gamma_c} N^A N^B n_i\,\mathrm{d}A d_i^A - \int_{\Gamma_c} M^A N^B n_i\,\mathrm{d}A d_i^A - \int_{\Gamma_c} N^B g \mathrm{d}A \right) \tag{18}$$

is the weighted mortar nodal gap. By using (15), this can also be written as

$$\delta^B = C_{Si}^{BA} d_i^A + C_{Mi}^{BA} d_i^A - g^B, \tag{19}$$

or in matrix notations as

$$\boldsymbol{\delta} = \boldsymbol{C}_S \boldsymbol{d} + \boldsymbol{C}_M \boldsymbol{d} - \boldsymbol{g}, \tag{20}$$

where $\boldsymbol{g}$ is a vector containing all initial gaps. The variational inequality in (17) must hold for any index B. Thus, the corresponding KKT conditions read

$$\boldsymbol{\lambda} \geq \boldsymbol{0}, \quad \boldsymbol{C}_S \boldsymbol{d} + \boldsymbol{C}_M \boldsymbol{d} - \boldsymbol{g} \leq \boldsymbol{0}, \quad \boldsymbol{\lambda} \circ (\boldsymbol{C}_S \boldsymbol{d} + \boldsymbol{C}_M \boldsymbol{d} - \boldsymbol{g}) = \boldsymbol{0}, \tag{21}$$

where $\circ$ represents the Hadamard product. These conditions are the same as the three latter conditions presented in (8) previously.

For any $r > 0$, and by also inserting (19), the inequality in (17) is equivalent to the following projection, see [3],

$$\lambda^B = \left(\lambda^B + r(C_{Si}^{BA} d_i^A + C_{Mi}^{BA} d_i^A - g^B)\right)_+. \tag{22}$$

By introducing $\boldsymbol{x} = \{\boldsymbol{d}, \boldsymbol{\kappa}, \boldsymbol{\lambda}\}$, using (22), (8) can be formulated compactly as

$$\boldsymbol{h}(\boldsymbol{x}) = \left\{ \begin{array}{c} \boldsymbol{K}\boldsymbol{d} + \boldsymbol{D}^T\boldsymbol{\kappa} + \boldsymbol{C}_S^T\boldsymbol{\lambda} + \boldsymbol{C}_M^T\boldsymbol{\lambda} - \boldsymbol{F} \\ \boldsymbol{D}\boldsymbol{d} - \boldsymbol{\delta} \\ -\lambda^B + \left(\lambda^B + r(C_{Si}^{BA} d_i^A + C_{Mi}^{BA} d_i^A - g^B)\right)_+ \end{array} \right\} = \boldsymbol{0}. \tag{23}$$

This equation system can be viewed as an augmented Lagrangian formulation. The standard approach is to solve this using Uzawa's algorithm, but in this work it is solved using the following Newton algorithm [3]:

Algorithm: Let $\beta_1 = 0.9$, $\beta_2 = 0.1$ and ϵ_{TOL} be a small value. Repeat the following steps:

0: Let $\boldsymbol{x}^0$ be a sufficiently good starting point and let $q = 0$.

1: Find a search direction $\boldsymbol{z}$ which satisfy

$$\boldsymbol{h}(\boldsymbol{x}^q) + \boldsymbol{J}(\boldsymbol{x}^q)\boldsymbol{z} = \boldsymbol{0},$$

where the Jacobian $\boldsymbol{J}(\boldsymbol{x}^q)$ is defined below.

2: Let $\alpha = \beta_1^m$, where m is the smallest integer $0 \leq m \leq 22$ which satisfies the following criterium:

$$\Phi(\boldsymbol{x}^q + \beta_1^m \boldsymbol{z}) \leq (1 - 2\beta_2\beta_1^m)\Phi(\boldsymbol{x}^q), \qquad \Phi(\boldsymbol{x}) = \frac{1}{2}\boldsymbol{h}^T(\boldsymbol{x})\boldsymbol{h}(\boldsymbol{x}).$$

3: Let $\boldsymbol{x}^{q+1} = \boldsymbol{x}^q + \alpha\boldsymbol{z}$.

4: If $\Phi(\boldsymbol{x}^{q+1}) \leq \epsilon_{\text{TOL}}$, then terminate with $\boldsymbol{x}^{q+1}$ as an approximate zero of $\boldsymbol{h}(\boldsymbol{x})$. Otherwise, update q with $q+1$ and return to step 1.

The Jacobian needed in the Newton algorithm above is defined by

$$\boldsymbol{J}(\boldsymbol{x})\boldsymbol{z} = \left\{ \begin{array}{c} \boldsymbol{K}\boldsymbol{z}_d + \boldsymbol{D}^T\boldsymbol{z}_\kappa + \boldsymbol{C}_S^T\boldsymbol{z}_\lambda + \boldsymbol{C}_M^T\boldsymbol{z}_\lambda \\ \boldsymbol{D}\boldsymbol{z}_d \\ \{-z_\lambda^B\}_{B\in\mathcal{J}_1} \\ \{r\{C_{Si}^{BA}z_{di}^A + C_{Mi}^{BA}z_{di}^A\}_{B\in\mathcal{J}_2} \end{array} \right\}, \tag{24}$$

where $\boldsymbol{z} = \{\boldsymbol{z}_d, \boldsymbol{z}_\kappa, \boldsymbol{z}_\lambda\}$,

$$\mathcal{J}_1 = \{B : \lambda^B + r(C_{Si}^{BA}d_i^A + C_{Mi}^{BA}d_i^A - g^B) \leq 0\},$$

and

$$\mathcal{J}_2 = \{B : \lambda^B + r(C_{Si}^{BA}d_i^A + C_{Mi}^{BA}d_i^A - g^B) > 0\}.$$

4 TOPOLOGY OPTIMIZATION FORMULATION

The total volume of bulk material generated in the assembly procedure is given by

$$V^{\text{bulk}} = V^{\text{bulk}}(\boldsymbol{\rho}, \boldsymbol{\gamma}) = \sum_e \rho_e\gamma_e V_e, \tag{25}$$

where V_e represents the total volume of each element e when $\rho_e = \gamma_e = 1$. By using (25), the design volume V^{design}, the volume of macro layout V^{macro} and the total volume of lattice in the design volume V^{lattice} are defined as

$$\begin{aligned} V^{\text{design}} &= V^{\text{bulk}}(\boldsymbol{1}, \boldsymbol{1}), \\ V^{\text{macro}} &= V^{\text{macro}}(\boldsymbol{\rho}) = V^{\text{bulk}}(\boldsymbol{\rho}, \boldsymbol{1}), \\ V^{\text{lattice}} &= V^{\text{lattice}}(\boldsymbol{\gamma}) = V^{\text{bulk}}(\boldsymbol{1}, \boldsymbol{\gamma}). \end{aligned} \tag{26}$$

Notice that the total volume of lattice in the design volume differs from the volume of lattice in the macro layout $V_{\text{macro}}^{\text{lattice}}$, which in turn is given by

$$V_{\text{macro}}^{\text{lattice}} = V^{\text{lattice}} - (V^{\text{design}} - V^{\text{macro}})l_b. \tag{27}$$

A more detailed discussion of these volume measures can be found in [1].

For the system presented in the two previous sections, the potential energy is maximized for separately constraints on the volume of macro layout, i.e. $V^{\text{macro}} \leq \hat{V}^{\text{macro}}$, and volume of lattice, i.e. $V^{\text{lattice}} \leq \hat{V}^{\text{lattice}}$, respectively, using a nested approach. That is,

$$\begin{aligned} &\max_{(\boldsymbol{\rho},\boldsymbol{\gamma})} \Pi(\boldsymbol{\rho},\boldsymbol{\gamma},\boldsymbol{d}(\boldsymbol{\rho},\boldsymbol{\gamma})) \\ &\text{s.t.} \begin{cases} V^{\text{macro}}(\boldsymbol{\rho}) \leq \hat{V}^{\text{macro}}, \\ V^{\text{lattice}}(\boldsymbol{\gamma}) \leq \hat{V}^{\text{lattice}}, \\ \epsilon \mathbf{1} \leq \boldsymbol{\rho} \leq \mathbf{1}, \\ l_b \mathbf{1} \leq \boldsymbol{\gamma} \leq u_b \mathbf{1}. \end{cases} \end{aligned} \tag{28}$$

The objective function in (28) can be interpreted by inserting the KKT-conditions from (8) into (1). This yields

$$\Pi(\boldsymbol{\rho},\boldsymbol{\gamma},\boldsymbol{d}(\boldsymbol{\rho},\boldsymbol{\gamma})) = -\frac{1}{2}\boldsymbol{F}^T\boldsymbol{d} - \frac{1}{2}\boldsymbol{\kappa}^T\boldsymbol{d} - \frac{1}{2}\boldsymbol{\lambda}^T\boldsymbol{g}, \tag{29}$$

implying that maximizing the potential energy is equivalent to minimizing

$$\boldsymbol{F}^T\boldsymbol{d} + \boldsymbol{\kappa}^T\boldsymbol{\delta} + \boldsymbol{\lambda}^T\boldsymbol{g}. \tag{30}$$

Here, the first term is the established compliance, the second term implies that the reaction force $-\boldsymbol{\kappa}$ is maximized for positive values on $\boldsymbol{\delta}$, and, finally, the third term implies that the mortar contact forces $\boldsymbol{\lambda}$ is minimized for positive initial contact gaps and maximized for $\boldsymbol{g} < \mathbf{0}$. Thus, for $\boldsymbol{g} = \mathbf{0}$ and $\boldsymbol{\delta} = \mathbf{0}$, the established compliance objective is recovered in (28).

The sensitivity analysis is carried out by introducing the corresponding Lagrangian

$$\mathcal{L}(\boldsymbol{\rho},\boldsymbol{\gamma},\boldsymbol{d},\boldsymbol{\kappa},\boldsymbol{\lambda}) = \Pi(\boldsymbol{\rho},\boldsymbol{\gamma},\boldsymbol{d}) + \boldsymbol{\kappa}^T(\boldsymbol{D}\boldsymbol{d} - \boldsymbol{\delta}) + \boldsymbol{\lambda}^T(\boldsymbol{C}_S\boldsymbol{d} + \boldsymbol{C}_M\boldsymbol{d} - \boldsymbol{g}). \tag{31}$$

At the state of equilibrium, defined by (8), this becomes

$$\mathcal{L} = \mathcal{L}(\boldsymbol{\rho},\boldsymbol{\gamma},\boldsymbol{d}(\boldsymbol{\rho},\boldsymbol{\gamma}),\boldsymbol{\kappa}(\boldsymbol{\rho},\boldsymbol{\gamma}),\boldsymbol{\lambda}(\boldsymbol{\rho},\boldsymbol{\gamma})) = \Pi(\boldsymbol{\rho},\boldsymbol{\gamma},\boldsymbol{d}(\boldsymbol{\rho},\boldsymbol{\gamma})), \tag{32}$$

which is utilized in the sensitivity analysis in the following manner:

$$\begin{aligned} \frac{\partial \Pi}{\partial \rho_e} &= \frac{\partial \mathcal{L}}{\partial \rho_e} = \frac{1}{2}\boldsymbol{d}^T\frac{\partial \boldsymbol{K}}{\partial \rho_e}\boldsymbol{d}, \\ \frac{\partial \Pi}{\partial \gamma_e} &= \frac{\partial \mathcal{L}}{\partial \gamma_e} = \frac{1}{2}\boldsymbol{d}^T\frac{\partial \boldsymbol{K}}{\partial \gamma_e}\boldsymbol{d}, \end{aligned} \tag{33}$$

because

$$\begin{aligned} \frac{\partial \mathcal{L}}{\partial \boldsymbol{d}} &= \boldsymbol{K}\boldsymbol{d} - \boldsymbol{F} + \boldsymbol{D}^T\boldsymbol{\kappa} + \boldsymbol{C}_S^T\boldsymbol{\lambda} + \boldsymbol{C}_M^T\boldsymbol{\lambda} = \mathbf{0}, \\ \frac{\partial \mathcal{L}}{\partial \boldsymbol{\kappa}} &= \boldsymbol{D}\boldsymbol{d} - \boldsymbol{\delta} = \mathbf{0}, \\ \left(\frac{\partial \mathcal{L}}{\partial \boldsymbol{\lambda}}\right)^T\frac{\partial \lambda}{\partial \rho_e} &= (\boldsymbol{C}_S\boldsymbol{d} + \boldsymbol{C}_M\boldsymbol{d} - \boldsymbol{g})^T\frac{\partial \lambda}{\partial \rho_e} = 0, \\ \left(\frac{\partial \mathcal{L}}{\partial \boldsymbol{\lambda}}\right)^T\frac{\partial \lambda}{\partial \gamma_e} &= (\boldsymbol{C}_S\boldsymbol{d} + \boldsymbol{C}_M\boldsymbol{d} - \boldsymbol{g})^T\frac{\partial \lambda}{\partial \gamma_e} = 0. \end{aligned} \tag{34}$$

The two latter equalities in (34) are a result from the last complementary condition in (8). In addition,

$$\begin{aligned} \frac{\partial \boldsymbol{K}}{\partial \rho_e} &= \frac{n+1}{(1+n(1-\rho_e))^2}\boldsymbol{k}_e(\gamma_e), \\ \frac{\partial \boldsymbol{K}}{\partial \gamma_e} &= \frac{\rho_e}{1+n(1-\rho_e)}\frac{\partial \boldsymbol{k}_e}{\partial \gamma_e} \end{aligned} \tag{35}$$

are inserted in (33), where $\partial f_{ij}/\partial \gamma_e$ also are needed.

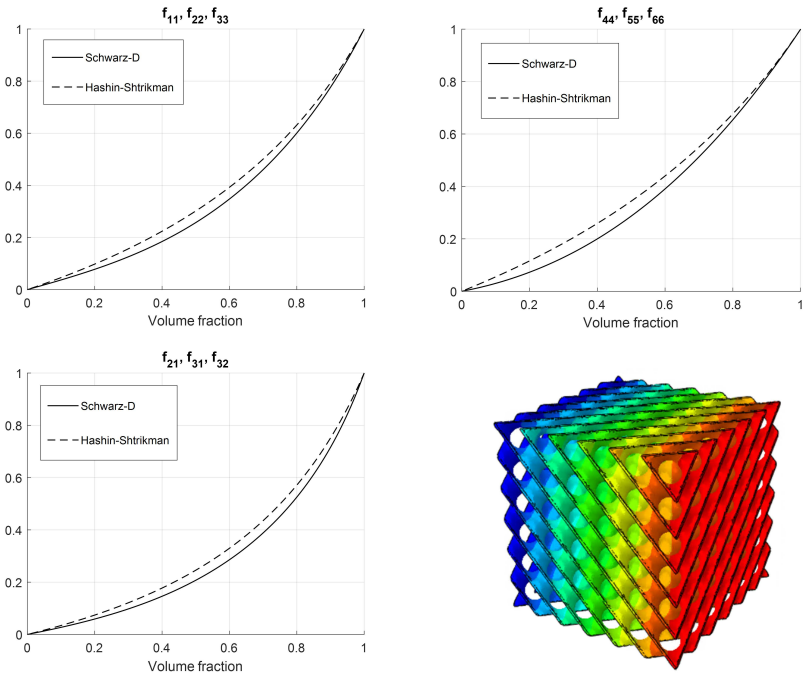

Figure 2: Material interpolation laws for the Schwarz-D lattice structure.

The sensitivities of the volume V^{macro} and V^{lattice} are

$$\frac{\partial V^{\text{macro}}}{\partial \rho_e} = \frac{\partial V^{\text{lattice}}}{\partial \gamma_e} = V_e. \tag{36}$$

The sensitivities with respect to both ρ_e and γ_e are treated using a linear density filter by applying the chain rule [10]. In addition, ρ_e is passing a smooth Heaviside filter [11].

Summarized, the sensitivity with respect to ρ_e in (33) is treated by the following formulas:

$$\begin{aligned}
\frac{\partial \Pi}{\partial \rho_e} &= \frac{\partial c}{\partial \rho_m^{\text{heav}}} \frac{\partial \rho_m^{\text{heav}}}{\partial \rho_m^{\text{filt}}} \frac{\partial \rho_m^{\text{filt}}}{\partial \rho_e}, \\
\rho_e^{\text{filt}} &= \frac{\sum_{g=1}^{n_{\text{el}}} \delta_g V_g \rho_g}{\sum_{f=1}^{n_{\text{el}}} \delta_f V_f}, \\
\delta_f &= \delta_f(e) = (r_{\min} - \text{dist}(e,f))_+, \\
\rho_e^{\text{heav}} &= \frac{\tanh(\beta\eta) + \tanh(\beta(\rho_e^{\text{filt}} - \eta))}{\tanh(\beta\eta) + \tanh(\beta(1-\eta))},
\end{aligned} \tag{37}$$

where $\text{dist}(e,f)$ denotes the distance between the center of element e and f, and $r_{\min}$ is the filter radius, which is set to 2 times the characteristic length of the finite elements in the numerical examples, η defines the threshold and β sets the slope of the smooth Heaviside filter. In the numerical examples, $\eta = 0.5$, β is ramped from 1 to 20, and the Heaviside filter is activated after 50 SLP iterations.

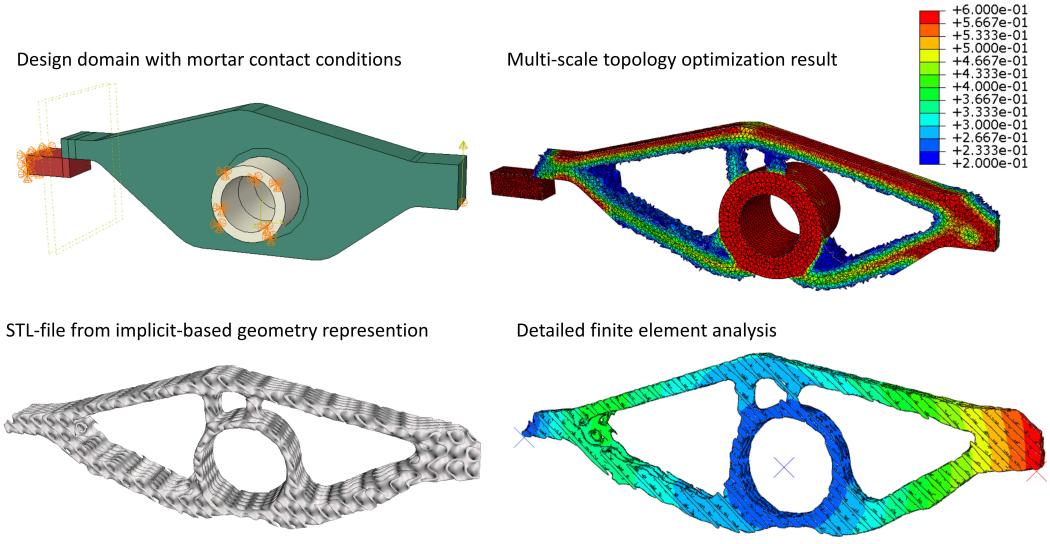

Figure 3: Topology optimization of a rocker arm with TPMS-based lattice structures and mortar contact conditions.

5 A NUMERICAL EXAMPLE

The multi-scale topology optimization approach for TPMS-based structures with mortar contact conditions presented in the previous sections is demonstrated in this section for shell-based Schwarz-D lattice with isotropic bulk properties, where Young's modulus is E=2.1E5 N/mm^2 and Poisson's ratio is ν=0.3. The material interpolation laws f_{ij} are established using numerical homogenization and the established laws are plotted in Figure 2 as well as the corresponding upper Hashin and Shtrikman bounds [12].

The demonstration is done for the rocker arm presented in Figure 3. The design domain is presented in green and mortar contact conditions are defined between the green and red parts, as well as the green and grey parts. The ends of the red support and the grey cylinder are fixed and the green design domain is subjected to an upward force at the right end. Furthermore, $l_b = 0.2$, $u_b = 0.6$, $\hat{V}^{\text{macro}} = 0.25$ and $V_{\text{macro}}^{\text{lattice}} = 0.4$. Thus, the total volume fraction of bulk material is only 0.1. The optimal solution is plotted at the upper right of the figure. This solution is then represented as an implicit-surface based geometry which in turn can be studied using detailed finite element analysis [13].

6 CONCLUDING REMARKS

In this paper, a multi-scale topology optimization framework for assemblies of TPMS-based lattice structures with mortar contact conditions is developed and implemented for 3D problems. The framework is most promising and next development would be to modify the formulation such that contact pressure also can be optimized.

REFERENCES

[1] Strömberg, N., A new multi-scale topology optimization framework for optimal combinations of macro-layouts and local gradings of TMPS-based lattice structures, *Mechanics Based Design of Structures and Machines*, on-line, 2022.

[2] Popp, A., Gee, M.W. and Wall, W.A., A finite deformation mortar contact formulation using a primal–dual active set strategy, *International Journal for Numerical Methods in Engineering*, **79**, 1354–1391, 2009.

[3] Strömberg, N., An augmented Lagrangian method for fretting problems, *European Journal of Mechanics, A/Solids* **16**, 573-593, 1997.

[4] Strömberg, N., An implicit method for frictional contact, impactand and rolling, *European Journal of Mechanics, A/Solids*, **24**, 1016-1029, 2005.

[5] Strömberg, N., An Eulerian approach for simulating frictional heating in disc-pad systems, *European Journal of Mechanics, A/Solids*, **30**, 673–683, 2011.

[6] Strömberg, N. and Klarbring, A., Topology optimization of structures in unilateral contact, *Structural and Multidisciplinary Optimization*, **41**, 57–64, 2010.

[7] Strömberg, N., Topology optimization of structures with manufacturing and unilateral contact constraints by minimizing an adjustable compliance-volume product, *Structural and Multidisciplinary Optimization*, **42**, 341-350, 2010.

[8] Stolpe, M. and Svanberg, K., An alternative interpolation scheme for minimum compliance topology optimization, *Structural and Multidisciplinary Optimization*, **22**, 116–124, 2001.

[9] Strömberg, N., Optimal Grading of TPMS-based Lattice Structures with Transversely Isotropic Elastic Properties, *Engineering Optimization*, **53:11**, 1871–1883, 2021.

[10] Bourdin, B., Filters in topology optimization, *International Journal for Numerical Methods in Engineering*, **50**, 2143–2158, 2001.

[11] Wang, F., Lazarov, B.S. and Sigmund, O., On projection methods, convergence and robust formulations in topology optimization, *Structural and Multidisciplinary Optimization*, **43**, 767–784, 2011.

[12] Hashin, Z. and Shtrikman, S., A variational approach to the elastic behavior of multiphase materials, *Journal of the Mechanics and Physics of Solids*, **11**, 127–140, 1963.

[13] Strömberg, N., Efficient detailed design optimization of topology optimization concepts by using support vector machines and metamodels, *Engineering Optimization*, **52**, 1136–1148 2019.